Verification Benchmarks and Validation of MAT261 for High Energy Dynamic Impact Applications

Matthew Molitor[1], Brian Justusson[2], Jaffar Iqbal[2], Alan Byar[2], Mostafa Rassaian[3]
The Boeing Company

Subject Category: Structures, Progressive Failure Analysis, High Energy Dynamic Impact

Advanced computational methods for composite structures can enable smarter testing and potentially certification by analysis. These methods, known as progressive damage and failure analysis (PDFA) methods, can predict lamina level mechanics including failure and subsequent propagation. When introduced into a commercial off the shelf finite element solver such as ABAQUS, LS-DYNA, or ANSYS, it enables end users to effectively exercise PDFA methods; however, it requires an understanding of the assumed mechanics and underlying coded response. In this paper, verification benchmarks developed under the NASA Advanced Composite Consortium for a class of PDFA methods known as continuum damage mechanics approaches are applied to the native LS-DYNA material model MAT261. As a result of the verification, an instability was discovered and subsequently corrected with an engineering solution. The results of the preliminary MAT261 simulations for high energy dynamic impact and the engineering solution are compared and a discussion about the significance is presented.

I. Introduction

The NASA Advanced Composites Consortium (ACC) High Energy Dynamic Impact (HEDI) team has been investigating Progressive Damage and Failure Analysis (PDFA) method applicability for discrete loading events such as fuselage shielding, fan blade containment, and bird strike [1]. PDFA material models have been developed that consider an in-plane material model coupled with an out-of-plane material (delamination) model. Effective use of these methods requires a detailed understanding of their formulation and of the material behavior at the formulation length-scale.

The HEDI Phase I team identified a number of promising PDFA approaches including MAT162, MAT261, and Peridynamics [2], [3]. As an established industry standard, MAT162 [4] was selected for its ability to account for material strain rate effects as well as localization effects through the inclusion of additional failure criteria related to fiber shear and fiber crush. MAT162, however, utilizes an advanced failure criteria (modified Hashin) for which it is difficult to fully determine input properties [5]. As such, the model relies on a number of calibration tests including the quasi-static punch shear test, low velocity impact, and others to set post-peak softening response. MAT162 also relies on a strength based delamination algorithm that does not require a strain energy release rate. These calibration parameters and strength based delamination capabilities generally limit predictive capability due to pathological mesh dependency.

MAT261 is a material model developed by Daimler and DYNAmore [6] and is commercially available in Livermore Software Technology Corporation's (LSTC) analysis tool, LS-DYNA [7] [8]. Within the context of the PDFA framework described by Schaefer and Razi [9], [10], [11] MAT261 is class-typical compared to other methods

---

[1] Structural Engineer, Boeing Research & Technology, 6300 James S. McDonnell Blvd. Berkeley, MO 63134, Non-Member.
[2] Structural Engineer, Boeing Research & Technology, 9725 East Marginal Way South, Tukwila, WA 98108, Non-Member
[3] Technical Fellow, Boeing Research & Technology, 9725 East Marginal Way South, Tukwila, WA 98108, AIAA Associate Fellow.

in the NASA ACC program [10] , the synthesis is quite similar (Figure 1). Like the Abaqus based Enhanced Schaper Theory (EST) and CompDam codes, MAT261 contains a pre-peak non-linear model and an energy based post-peak response. This energy based post-peak response is a result of the inclusion of a traction separation law that eliminates the pathological mesh dependency by regularizing the energy based on the characteristic element length. MAT261 also includes a 3D LaRC-04 failure criteria [12]. The LaRC-04 failure criteria takes advantage of transverse isotropy assumptions such that if a ply is loaded through the thickness (e.g. the 1-3 plane) the response is the same as the in-plane direction for matrix failure. In this regard, it differs from MAT162 in that it does not include specific fiber crush and fiber shear failure modes.

From Figure 1, the MAT261 model contains all of the capabilities of a state-of-the-art method for in-plane and out-of-plane behavior when coupled with LS-DYNA's native tie-break contact. In this work, benchmarks are evaluated to establish best practices for MAT261 implementation for modeling HEDI events. After combining the lessons learned and best practices with the standard verification of the in-plane material model [13], MAT261 is validated with a uniform flat composite panel subject to a high energy impact test.

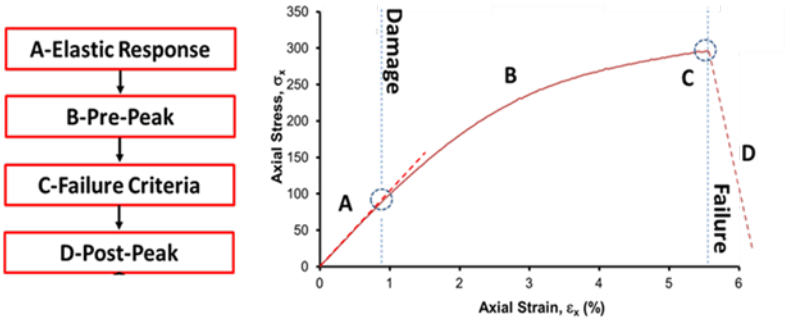

Component	MAT162	MAT261	Peridynamics	CompDam	EST
Method Class	Continuum Lamina	Continuum Lamina	Discrete/Enriched	Continuum Lamina	Continuum Lamina
A. Elastic Response	3D Elastic	3D Elastic	3D Elastic	3D Elastic	2D Elastic
B. Pre-Peak	None	Shear non-linearity (tabular data)	None	Ramberg-Osgood shear non-linearity	Schapery microdamage
C. Failure Criteria	Modified Hashin, Mohr Columb	LARC-04	Critical Bond Stretch	LARC-04 (Stress basis)	Hashin-Rotem (Strain basis)
D. Post Peak	Softening Parameters	3D Crack band	None	3D Crack band w/DGD	2D Crack band

Figure 1. Comparison of MAT261 to other PDFA methods using the Schaefer framework [9]

II. Verification of MAT261 Material Card

The MAT261 verification pathway is shown in Figure 2. This verification pathway incorporates the lessons learned on the NASA ACC Phase I program for intralaminar and interlaminar benchmarking and has been modified for the LS-DYNA framework. For LS-DYNA methods, the top row are all dependent on material properties that are used for the simulations. The first two cases to be studied are the center notch tension (CNT) and center notch shear (CNS) cases for intralaminar failure modes. The delamination cases are built based on tie-break contact. The following is a concise description of each of the benchmark problems:

1. **Center Notch Tension (CNT):** A notch is placed in the center of an infinite single ply plate with pure tension applied in-plane, 90° transverse to the fiber direction. The notch height is set equal to one row of elements and the far field stress at which the load drop is observed is compared to a linear elastic fracture mechanics (LEFM) solution for a range of mesh sizes. This benchmark ensures self-similar growth of matrix cracks is physically relevant and establishes a range of applicable mesh sizes.

2. **Center Notch Shear (CNS):** A notch is placed in the center of an infinite single-ply plate with pure shear applied in the plane of the lamina. The notch height is set equal to one row of elements and the far field stress at which the load drop is observed is compared to a LEFM solution for a range of mesh sizes. This benchmark ensures self-similar growth of matrix cracks is physically relevant and establishes a range of applicable mesh sizes.
3. **Mode I Delamination**: Tie-break contact is used between two loading arms that are subjected to mode I (opening) forces. The load-deflection response is compared to test data for a double cantilevered beam (DCB) test. The cohesive strength is varied as a function of mesh size to ensure appropriate propagation behavior.
4. **Mode II Delamination**: Tie-break contact is used between two loading arms that are subjected to three point bend loading to induce a mode II delamination. The load-deflection response is compared to test data for an end notch flexure (ENF) test. The cohesive strength is varied as a function of mesh size to ensure appropriate propagation behavior.
5. **Mixed Mode Delamination**: Tie-break contact is used between two loading arms that are subjected to three point bend loading to induce a mode II delamination combined with mode I. The load-deflection response is compared to test data for a mixed mode bending (MMB) test. This test ensures the appropriate mixed mode delamination law is appropriately accounted for.

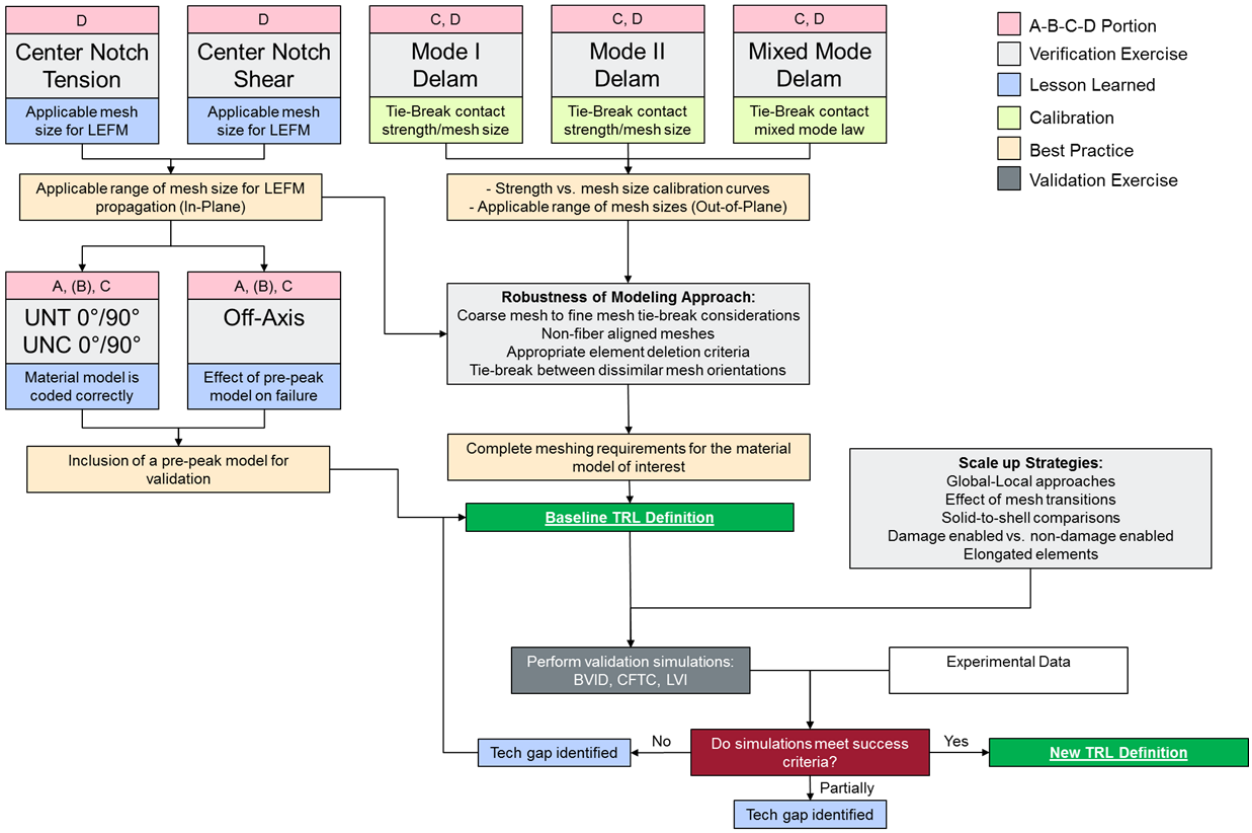

Figure 2. Verification pathway for MAT261 implementation

The next part of the verification examines the pre-peak response of the material model through single element verification. This is performed in two parts: (1) load an element in the material coordinate systems in the fiber and matrix direction and (2) off-axis by changing the direction of the fibers with respect to the applied load. Performing the off-axis tension and compression sweeps verifies that the code is determining the appropriate failure envelope for combinations of in-plane tension/compression and shear. The off-axis simulations can also be used with and without shear non-linearity to ensure that the inclusion of shear non-linearity does not affect the recovery of the failure envelope. Of note, these are not compared to test data and only to analytical solutions.

Best practices determined as a result of verification were applied to the subsequent modeling phase. These best practices include:

1. Modeling is performed at the lamina length scale, ensuring that each ply is modeled as a single element through the thickness.
2. Fiber aligned meshing is used for all plies. This is a requirement for fracture based CDM approaches in which a fracture energy is calculated from a characteristic element length [14].
3. The selected mesh size conforms to the limits established from the CNT and CNS benchmark.
4. Tie-break contact is used between all plies to model delamination.
5. The cohesive strengths used for tie-break contact are determined for the mesh sizes used in the model by comparing results to mode I and mode II interlaminar fracture tests.

III. Validation Testing of Impact Panels

Validation testing was performed on a uniform flat panel. The test articles have no structural features and are 25" x 25" flat panels as shown in Figure 3. Flat panels were fabricated from IM7/8552 uni-directional tape (nominal thickness of 0.0072"/ply) using a standard cure profile recommended by the manufacturer. The panels were a twenty-four ply quasi-isotropic laminate (i.e. $[45/90/-45/0]_{3S}$). The panels were fabricated by Boeing and provided to NASA Glenn Research Center (GRC) for impact testing.

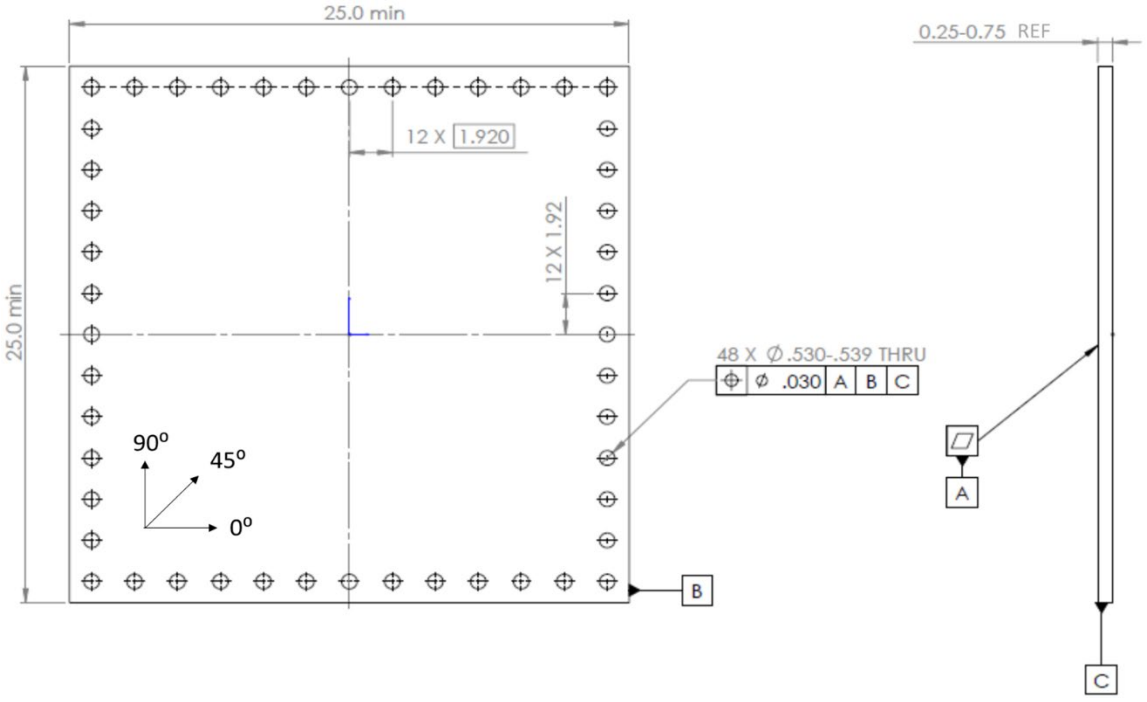

Figure 3. Schematic of Flat Panel Only test article

NASA GRC utilized the same test fixture that was used in Phase I, a schematic of which is shown in Figure 4 [15]. The panel was mounted between two square frames and held securely along the edges of the test article. Holes were drilled in the panel such that they are normal to the test frame in the setup. There were four (4) total load cells positioned behind the mounting frame, one at each of the corners. These load cells were ring shaped and were dynamically rated for impact. The load cell was preloaded by passing a bolt through the middle and tightening to 16 kips.

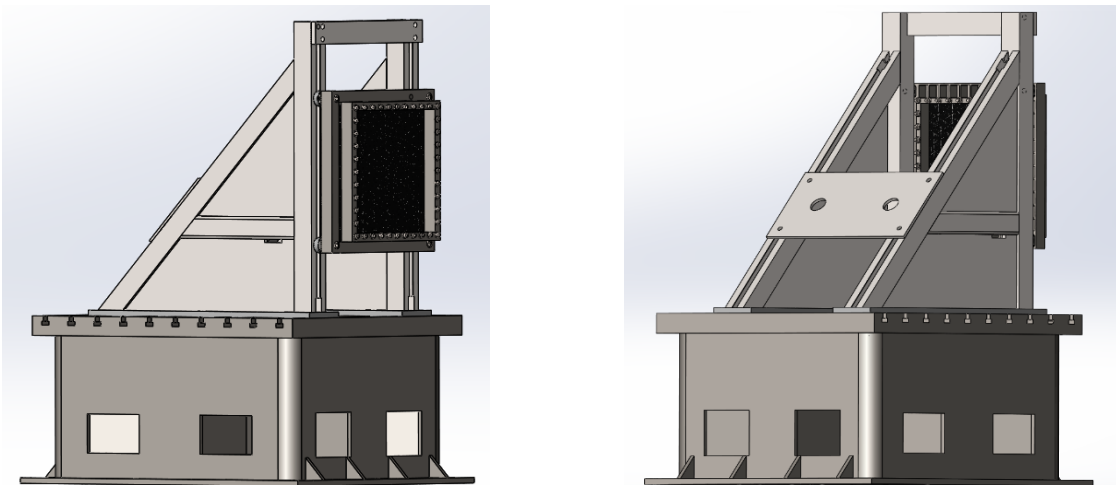

Figure 4. Overview of the NASA GRC impact test fixture

Impact testing used the projectile typical for Phase II of the program [1]. The projectile was an Al-6061 semi-hollow cylinder with approximately 2" diameter, 1.95" length and a 1.5" radius rounded nose. Figure 5 shows an image of the projectile. The projectile has the same outside geometry as the ASTM standard D8101 [16]. The nose and walls are thicker than the ASTM standard, and maintain a smoother thickness transition between nose and walls. The Phase II projectile also differs in weight at 90 grams, compared to 50 grams for the ASTM standard D8101.

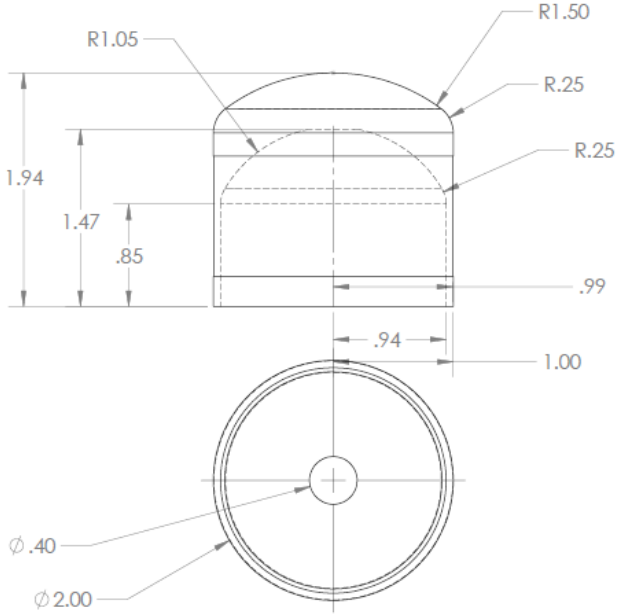

Figure 5. Schematic of the ACC HEDI phase II projectile (Dimensions in inches)

The projectile was shot at a series of identical test panels using a single stage gas gun (L=23 feet, D=2 in.) at prescribed velocities until the ballistic limit of the target was determined. As the projectile was airborne, a photogate triggered a set of stereo high-speed DIC cameras to measure the deflection-time history of the panels. The ballistic limit and testing was performed in accordance with the ASTM D8101.

Impact tests were successfully performed at NASA GRC. Eight (8) 24-ply were impacted with the Phase II projectile at a variety of impact velocities ranging from 280 – 610 ft/s. Digital photogrammetry was used to collect a variety of data including panel deflection, strain response, and projectile velocity. Post-test imaging and non-destructive inspection (NDI) were used to further examine the test articles for damage and delamination. A sample of the damage and delamination in a typical impacted panel is shown in Figure 6.

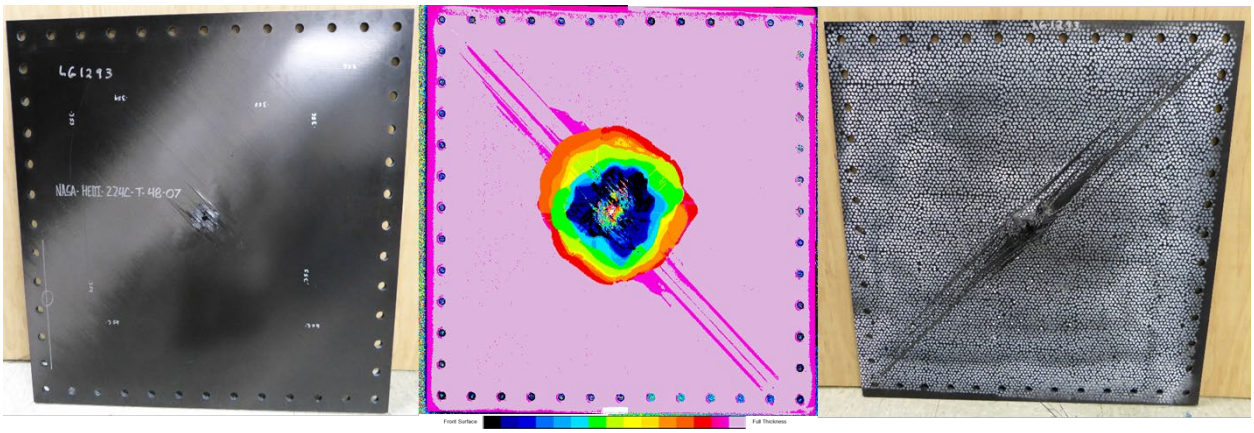

Figure 6. Post-test damage of impacted panel (a) front face, (b) NDI scan, and (c) back face

IV. Preliminary Validation Attempts with MAT261 Using Best Practices

Using LS-DYNA to simulate the impact tests performed by NASA GRC, MAT261 was used to model the flat panel test article. The simulation setup is shown in Figure 7. In the HEDI program, 24 ply laminates were impacted. The laminates were modeled using the previously described best practices. The test fixture was modeled as two frames clamped around the periphery with a uniform pattern of preloaded bolts. The bolts were prescribed a tension preload using dynamic relaxation. The load cells are also modeled in the same position as the experiment. Phase I simulations showed this model to be an appropriate simulation of the test setup [3], ensuring the use of validated boundary conditions. The Phase II projectile is modeled using a validated MAT098 (Simplified Johnson-Cook) material card [1] based on the work of Manes et al. [17].

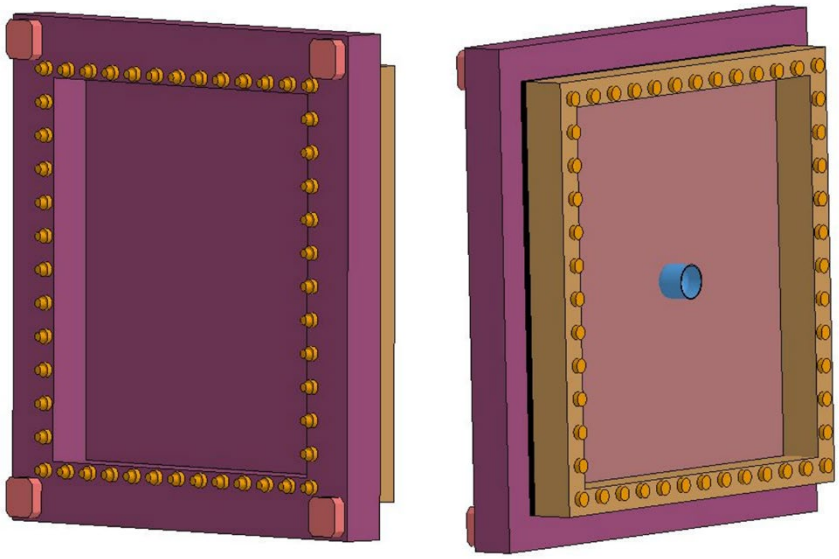

Figure 7. LS-DYNA impact simulation overview

Figure 8 lists the material properties and input parameters for MAT261 [6]. Based on the verification results, it was determined that the PFL, PUCK, and SOFT parameters are not applicable for use with Element Form 1 solid elements in LS-DYNA. PFL is a parameter that is used with shell elements that relates the percentage of failed layers to when integration points are deleted. PUCK is a flag that is used to evaluate if the PUCK intrafiber failure criteria is

met, but does not change the simulations. SOFT is used to modify the strength of elements located in a crash front, and would violate established best practices for the current approach. Since these input parameters are deactivated, the fully populated MAT261 material card has no calibration parameters in use. Each of the input properties are directly taken from experimental values generated in Phase I. Of note, two parameters require further consideration:

1. EFS is the equivalent failure strain which triggers element erosion. This value should be set sufficiently high such that it does not erode an element that is currently going through the fracture energy release process. If an element is eroded prematurely due to triggering EFS during the traction-separation law of the element constitutive model, the failure process zone never fully develops. As such, fracture based propagation does not occur depending on the selection EFS. For this work, EFS was effectively minimized by ensuring that it was sufficiently large to not affect the traction-separation law. The elements are able to delete when artificially high strains are met.
2. LCSS is a load curve ID. The load curve that is used for this is generated from the in-plane shear test and is input as a true shear stress-strain curve. If used, this stress-strain input overrides the definition of the constant in-plane shear modulus material property, GAB. This data was generated as part of the Phase I efforts.

		1	2	3	4	5	6	7	8
elastic properties	Card 1	MID	RO	EA	EB	EC	PRBA	PRCA	PRCB
	Card 2	GAB	GBC	GCA	AOPT	DAF	DKF	DMF	EFS
material coordinates	Card 3	XP	YP	ZP	A1	A2	A3		
	Card 4	V1	V2	V3	D1	D2	D3	MANGLE	
material parameters and strength	Card 5	ENKINK	ENA	ENB	ENT	ENL			
	Card 6	XC	XT	YC	YT	SL			
	Card 7	FIO	SIGY	LCSS	BETA	PFL	PUCK	SOFT	

DAF: flag to control failure of an IP based on longitudinal (fiber) tensile failure
DKF: flag to control failure of an IP based on longitudinal (fiber) compressive failure
DMF: flag to control failure of an IP based on transverse (matrix) failure
EFS: Max. effect. Strain for element layer failure. A value of unity would equal 100% strain
ENKINK: Facture toughness for longitudinal (fiber) compressive failure mode
ENA: Facture toughness for longitudinal (fiber) tensile failure mode
ENB: Facture toughness for intralaminar matrix tensile failure
ENT: Fracture toughness for intralaminar matrix transverse shear failure
ENL: Fracture toughness for intralaminar matrix longitudinal shear failure
XC: longitudinal compressive strength
XT: longitudinal tensile strength
YC: transverse compressive strength
YT: transverse tensile strength
SL: longitudinal shear strength
FIO: fracture angle in pure transverse compression (in degrees, default=53.0)
SIGY: In-plane shear yield stress
LCSS: Load curve ID which defines the non-linear in-plane shear-stress as a function of in-plane shear-strain
BETA: hardening parameter for in-plane shear plasticity
PFL: Percentage of layer which must fail before crashfront is initiated.
PUCK: flag to post-process Puck's inter-fiber-failure criterion
SOFT: reduction factor for strength in crashfront elements

Figure 8. MAT261 material property and input parameter definitions [8]

In the model, the projectile was initialized slightly offset from the surface in the center of the laminate and prescribed an initial velocity. The model tracked the projectile velocity to determine the energy dissipation capabilities of the panel. Simulations were run to a point such that projectile penetration or rebounding could be determined. Penetration events were characterized by an asymptotic approach to a finite velocity above zero. Rebound events were characterized by evaluating the slope of the velocity curve as it reaches zero velocity.

The preliminary model was run at a velocity of 3600 in/s, a velocity experimentally shown to be below the test panel V50. The velocity profile of the projectile is shown in Figure 9, which shows that it is asymptotically approaching a value which is characteristic of a penetration event with a residual velocity of approximately 2750 in/s. Calculating the difference in kinetic energy shows that the composite dissipated only 41% of the energy if plastic deformation of the projectile is not considered.

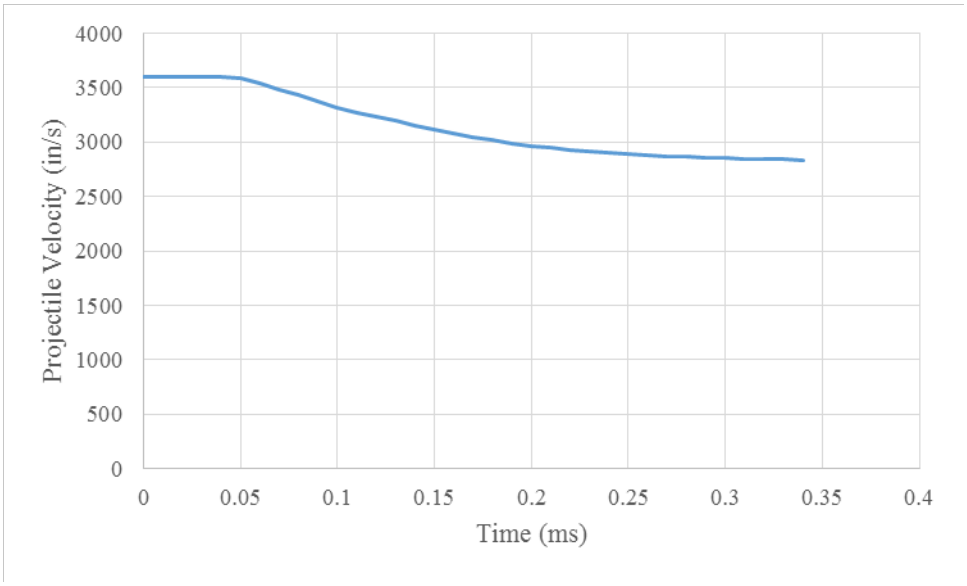

Figure 9. Projectile velocity-time history for impact vs 24 ply panel for the preliminary model

Figure 10 shows the matrix damage predicted by the preliminary model within the panel for the baseline MAT261 formulation. In the contour plots, the elements with a value of 1.00 have met the stress limit criteria for matrix damage (HistVar 3) and have entered the post-peak strain softening portion of the traction separation behavior. As seen in the image, the damage is relatively limited to the region under the impactor and does not extend out as observed in the experiment (Figure 6). This is consistent with the other finding that the energy dissipation in the panel was minimal.

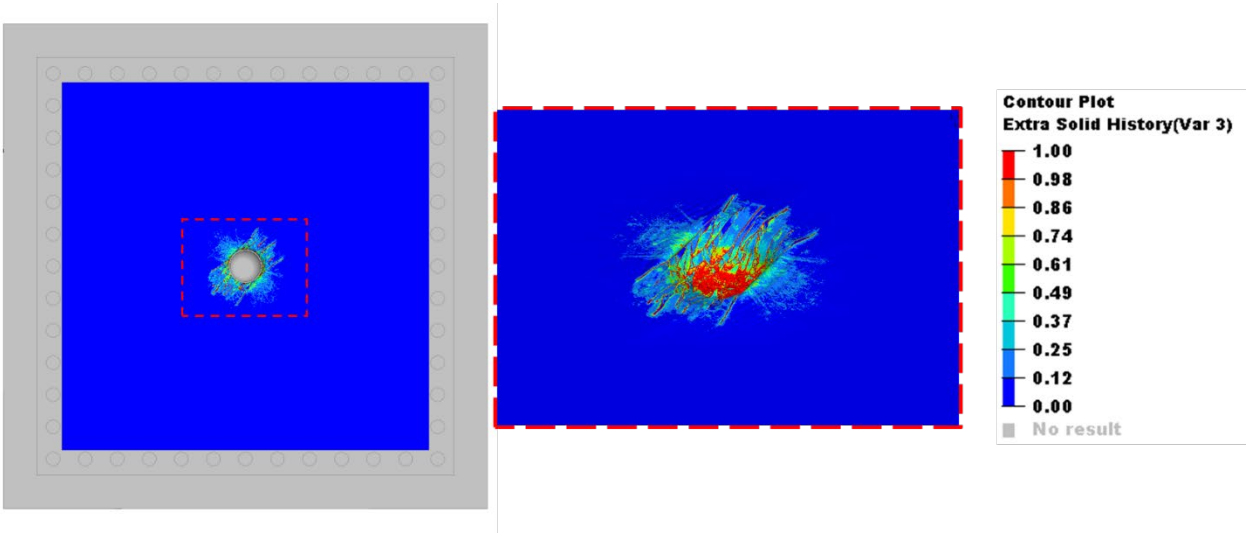

Figure 10. Predicted damage morphology of the panel impact using baseline MAT261 model

Figure 11 shows the fully developed matrix cracks predicted by MAT261. The extent of the cracks is generally within one diameter of the projectile. While not explicitly shown, this can also be a de facto measure of the projected delamination area. This is because delamination in CDM approaches generally is led first by matrix cracks and the extent of the delamination is bounded significantly within these regions. Of note, when running this model there were large reductions in the stable time increment leading to long model run times. Eventually this lead to a fatal element instability that will be discussed in the next section.

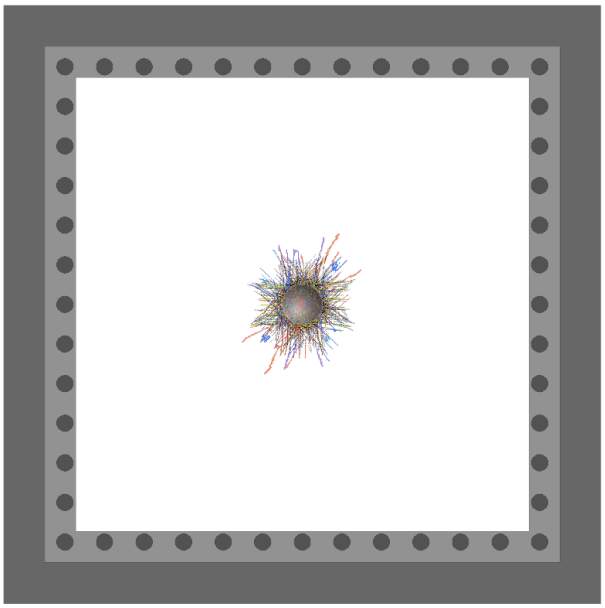

Figure 11. Fully developed matrix cracks predicted by the baseline MAT261 model

V. Development of Engineering Solution for Element Stability

The instability that was observed within the material model can be directly explained from the results of single element verification and subsequently validated as an instability in a multi-element model. MAT261 includes native flags to the material model called DAF, DKF, and DMF which remove the element from the model when the prescribed fracture energy in the post-peak response is completely dissipated for longitudinal (fiber) tension, compression, and transverse (matrix) failure, respectively. In order to maintain model stability after a matrix failure, the DMF flag can be activated to remove the element from the simulation. Removing elements due to matrix failure during HEDI events is a poor approximation of the material behavior and is inherently non-physical. While the matrix may be damaged to the point of failure, the fiber still has the ability to carry load under membrane loading which warrants the retention of the matrix-failed element

The single element verification to demonstrate the effects of the erosion flags is shown in Figure 12. In this case, the DMF flag is set to 0, and the element is intended to erode. The single element was loaded with tension in the transverse direction. Under the monotonic loading, when the stress reaches the YT stress limit for the transverse tension failure criteria, the element begins to follow the traction-separation law and experiences strain-softening. When multiplied by the element volume, the area under the resulting stress-strain curve is equal to the fracture toughness input property, ENL. Once the energy is fully dissipated, the element erodes from the model as shown in Figure 12. If the DMF flag is switched to a value of 1.0, the element remains in the model. Best practices indicate that the continuum should be maintained as long as possible in order to avoid the removal of energy from the model.

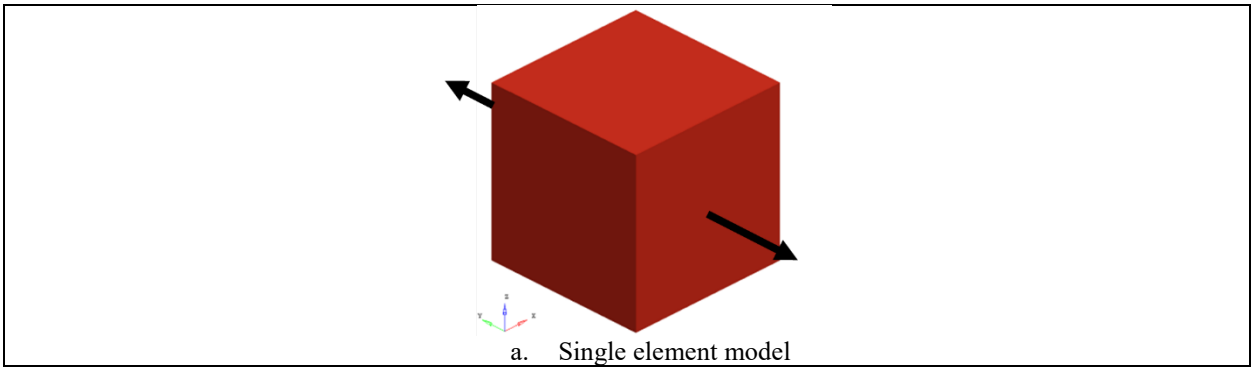

a. Single element model

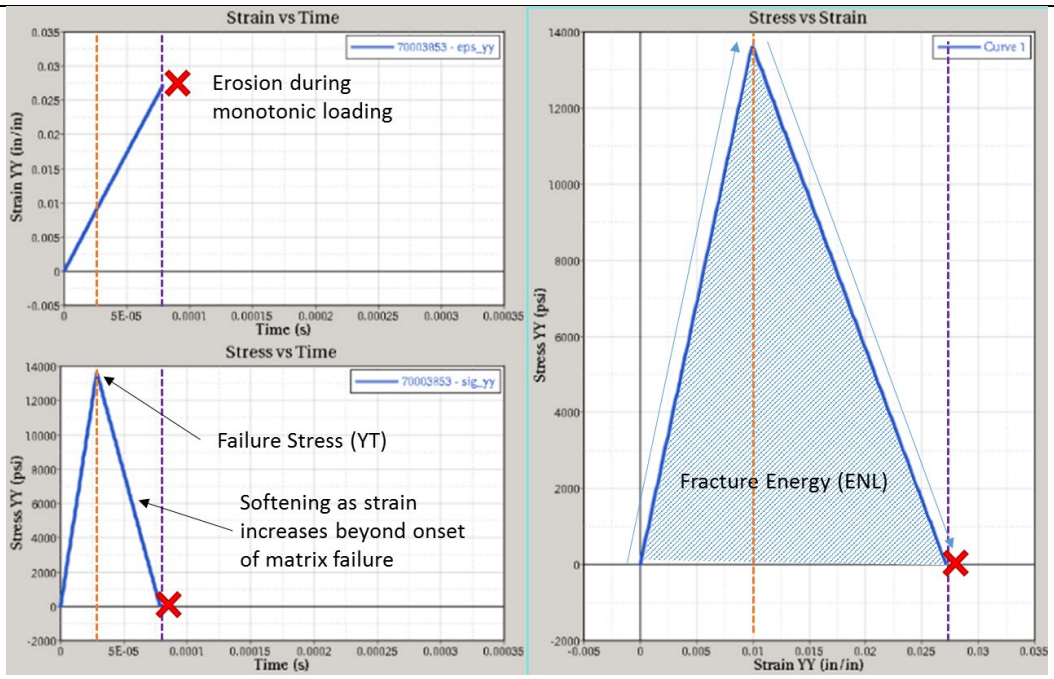

b. Element histories

Figure 12. Single element verification with DMF flag set to 0 (element erodes)

When the element remains in the model (DMF=1.0), the element maintains zero stiffness in all matrix dominant directions. With zero stiffness in multiple directions, the element has no ability to resist applied strains/displacements and quickly distorts to numerically unstable shapes. While a single element material model might not present a particular problem, when put into a larger model, the effect is more apparent. To demonstrate this effect, a five element model was created. The five element model was subjected to two different steps. In step one, the elements were subjected to transverse tensile loading. The loading was sufficient enough to cause the model to fully dissipate the energy associated with fracture toughness input property and to show zero residual stiffness. The elements were then returned to a zero strain condition. The elements were then pulled in the axial direction (fiber tension) and the stress-time history was recorded. At approximately 50 ksi, one element began to show stability issues which lead to model termination due to a fatal error. This value is less than 15% of the fiber strength (XT) input property of the material model.

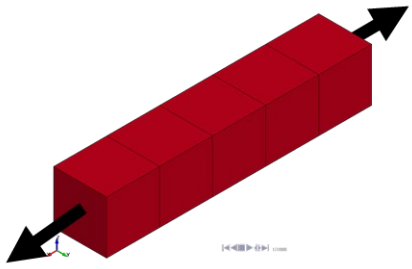

a. Five element model

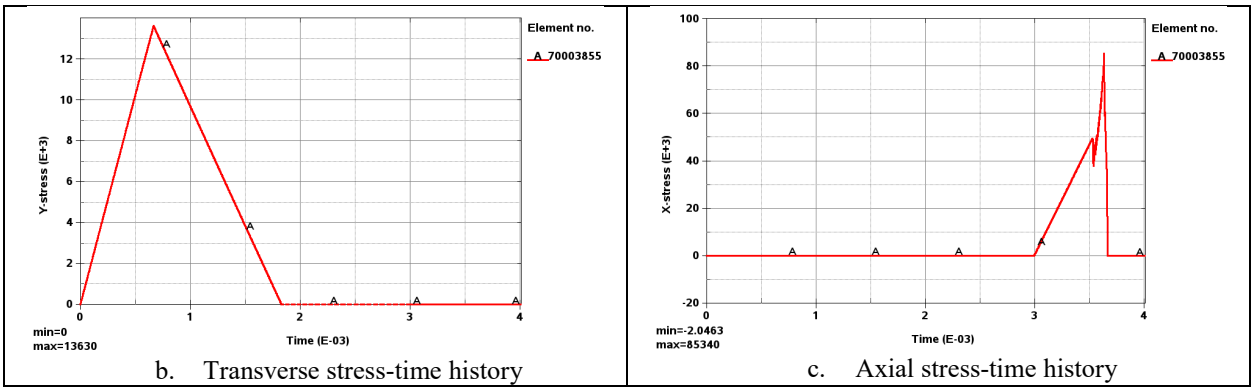

b. Transverse stress-time history c. Axial stress-time history

Figure 13. Example model setup and results demonstrating five element verification

In order to continue analysis, improved stability of a failed element was needed. The issue was communicated to LSTC, the developer of LS-DYNA, and an engineering approach was developed. In this engineering approach, it allowed the user to take advantage of traditional CDM damage models that calculate the damage variable, D. The damage variable can be used in conjunction with a stiffness, k, to develop a modified slope of the unloading curve (Figure 14). As damage develops, the variable increases closer to a value of one. Subsequently, the slope of the unloading curve is reduced. With the engineering approach, the user now has the ability to set the flag parameter for any of the failure modes to a non-binary integer between 0 and 1. The value represents how much the damage variable is allowed to develop before additional damage is prevented from occurring. For example, if a flag is set to 0.25, the damage variable can only develop 25% and will follow the loading/unloading curve shown in Figure 14. This approach showed improved stability in the five element model and was used for validation against the impact test article presented previously.

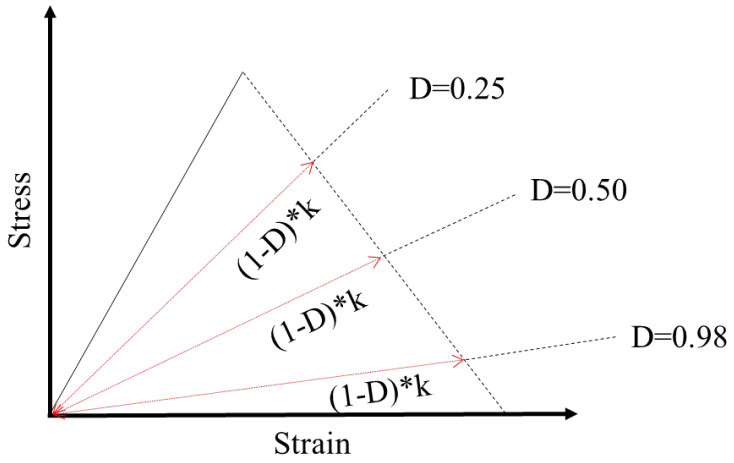

Figure 14. New DMF, DKF, and DAF flag capability defines the lower limits of residual stiffness in failed elements

VI. Validation Attempts with Improved Stability of MAT261

The enhanced model used all the same modeling practices as previously described in the evaluation of the preliminary model. Guided by experimental data, an impact velocity of 4200 in/s was used for the enhanced model. Recall that in the preliminary run, a lower 3600 in/s velocity was shown to be well above the V50 limit of the panel and indicated easy penetration of the original MAT261 model. The same input decks were used with the updated MAT261 with the DMF flag set to a value of 0.98. This value was selected in order to allow the matrix damage process zones to fully develop and because it was used in the lower level validation models. This approach ensures a nominally small stiffness in the model to maintain element stability to transfer stress in other directions after matrix failure.

Figure 15 shows a curve that is characteristic of a penetration event that has a low residual velocity. The velocity profile indicates that it is asymptotically approaching a small positive value which is results in a penetration event with a small residual velocity <500 in/s. This shows a significant stability improvement compared to the original model, which further allows for greater dissipation of the projectile kinetic energy into the panel. Calculating the difference in kinetic energy shows that the composite dissipated approximately 99% of the energy if plasticity in the projectile is not accounted for.

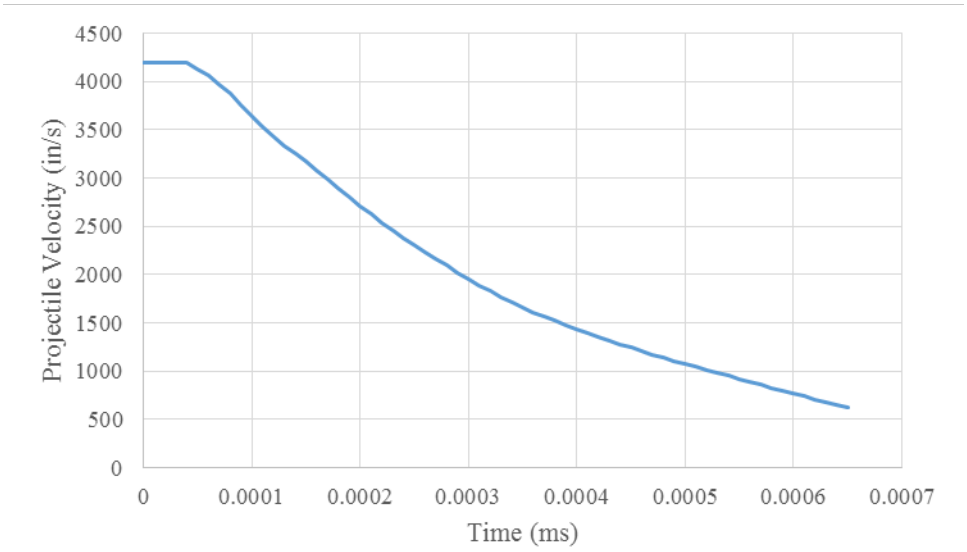

Figure 15. The velocity-time profile of the projectile with the MAT261 engineering approach

Figure 16 shows the extent of matrix damage predicted by the model within the panel for the enhanced MAT261 formulation. In the contour plots, the elements with a value of 1.00 have met the stress limit criteria for matrix damage (HistVar 3) and have entered the post-peak strain softening portion of the traction separation behavior. The area surrounding the point of impact shows a significant increase in the extent of damage within the panel material. The damage morphology extends along the fiber directions within each lamina as observed in the experiment. Further the damage plot shows more cracks within the material. Figure 17 shows the extent of the fully developed cracks within the material overlaid through the thickness of the panel. The matrix cracks follow the lamina fiber directions and have developed much further from the point of impact in comparison to the preliminary model.

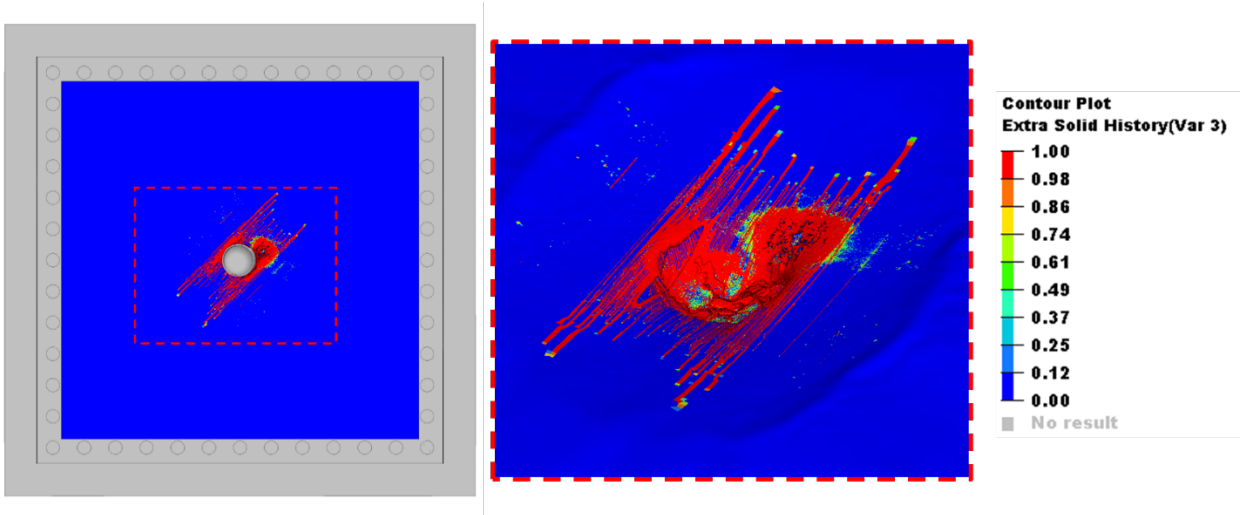

Figure 16 . Predicted damage morphology of the panel impact using updated MAT261 model

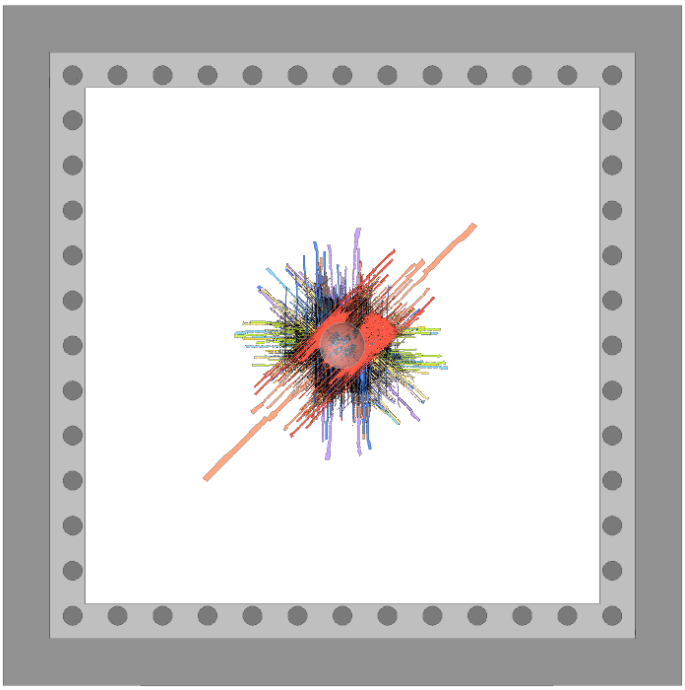

Figure 17. Fully developed matrix cracks predicted by the updated MAT261 model

VII. Discussion

The damage-limiting enhancement to MAT261 enabled improved stability within the material model; however, it is still an engineering approximation. The selection of the erosion flag values prescribes the lower limit of residual stiffness within the elements. This approximation is significant because MAT261 has three modes of failure: fiber tension, fiber compression, and matrix. The limitation of the current formulation is that once the matrix has failed (e.g. in matrix tension), the element lacks the residual stiffness to maintain stability. The element still has the ability to carry load in the fiber direction, however, the lack of a nominal residual shear stiffness leads to fatal element instability. With the improvements, MAT261 now allows the fibers to continue to transfer load after significant matrix damage occurs through the use of a residual stiffness limit. However, the effectiveness of the fibers remains limited in specific loading conditions as the nominal residual stiffness of the matrix is not great enough to effectively transfer load to the fibers.

Figure 18 compares the original model, the enhanced model, and an ultrasonic non-destructive image (NDI) that shows a characteristic damage state within an impact test panel. Comparing Figure 18a and 18b, the extent of matrix failure in the model has poor agreement with the NDI. The load path necessary to continue to load fibers after the matrix has failed does not exist, which explains the localization of the damage. As such, matrix damage accumulates in a local volume until fatal element instability occurs. The limitation of this approach is that the reduction in stiffness reduces the critical time step within the simulation, greatly increases the model run time, and eventually leads to fatal model errors. When comparing Figure 18b to c, there is much better agreement with the damage state observed by the NDI. The improvement to MAT261 allows for the development of the far-field matrix cracks because load can now be carried along the fibers.

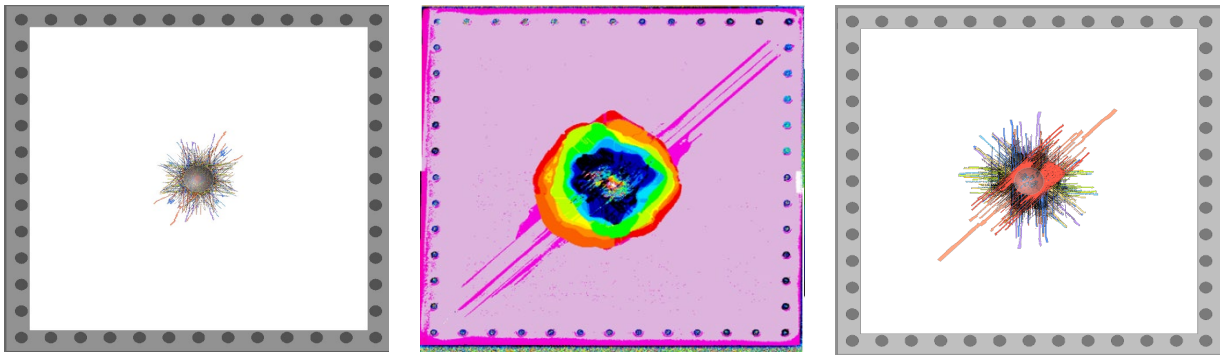

a. Original Run b. NDI Image of characteristic damage state c. Improved MAT261

Figure 18. Demonstration of improved damage state prediction in comparison

Another indication of the improved capability is the conservation of total energy within the model. With many CDM approaches, element erosion (or deletion) can be a significant mechanism by which model behavior is altered. However, the erosion of elements results in the removal of energy from the model as each element has an associated kinetic and internal energy. Therefore, with CDM approaches, the continuum should be maintained for as long as possible meaning that elements should only be removed if required for model stability. Within the LS-DYNA framework, there are four (4) primary types of energy that must be considered for computational equilibrium including internal energy, kinetic energy, contact energy, and hourglass energy. Best practices maintain how hourglass stability should be controlled during the model, ensuring the contribution to total model energy is small. When these energies are summed, the total energy should remain constant during the course of the simulations. To keep the model as physically relevant as possible, the eroded energy should be minimized.

Figure 19 shows the total energy ratio as a function of time for both the preliminary and the improved MAT261 impact models. The initial total energy of the model was equal to the initial kinetic energy of the projectile. At each data point, the hourglass, contact, kinetic, and internal energies are summed and normalized by the initial total energy. Any deviation from a value of 1.0 indicates that energy was eroded from the model. At the point of model termination, the original model had eroded approximately 4% of the total initial energy. By comparison, the updated MAT261 model eroded less than 0.5% of the initial energy for the same mesh. The updated model remained stable through the duration of the run enabling the completion of the simulation. Also, the updated MAT261 model used an initial projectile velocity of 4200in/s compared to the original model which used 3600in/s. This improved energy conservation highlights the ability of the updated model to effectively dissipate large amounts of kinetic and internal energy through the formation of material damage away from the immediate area of impact, which is enabled by the improved element stability through the use of residual stiffness limits.

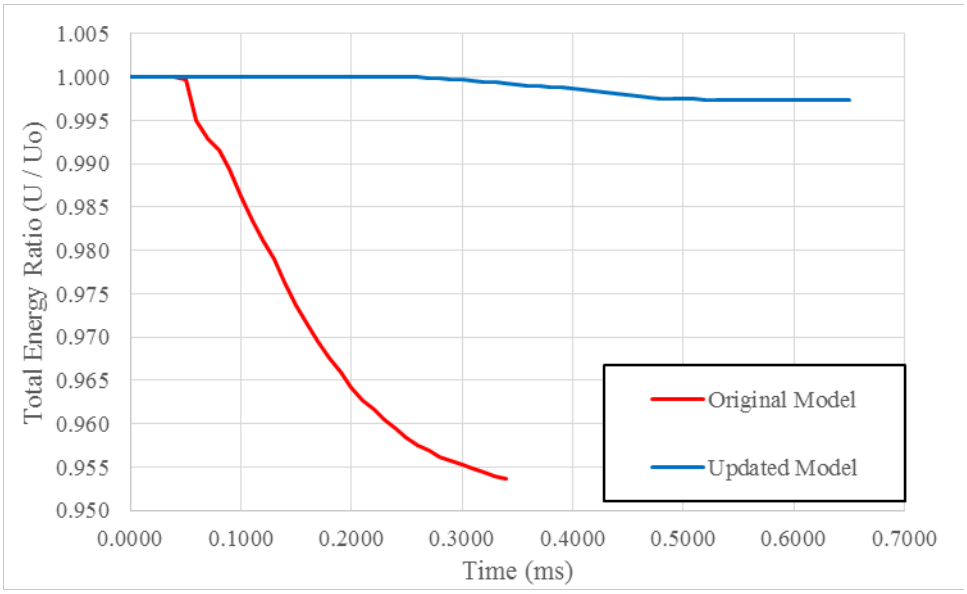

Figure 19. Comparison of energy ratio between both models

VIII. Summary

A high energy dynamic impact (HEDI) event was simulated using MAT261, a progressive damage and failure analysis material model available in the LS-DYNA explicit finite element analysis solver. Using an efficient framework for verification, MAT261 was studied to understand the piecewise formulation of the material model. Best practices were carried forward and a HEDI test event on a flat panel was studied with the current MAT261 material model. The simulation showed that the model was not dissipating energy appropriately to enable predictive capability, and frequently resulted in model instability. Using the simple failure modes, Boeing and LSTC partnered to implement an engineering solution that allowed for a residual stiffness to be maintained in the material model after matrix failure. The initial models were rerun with the enhanced version of MAT261 and showed improved correlation to V50 results as and to the predicted damage morphology. It was concluded that the enhancements to MAT261 improved the model stability. The updated MAT261 formulation was used for the duration of the NASA HEDI program with reasonable correlation with test data for a variety of test articles.

IX. Acknowledgements

The material is based upon work supported by NASA under Award Nos. NNL09AA00A and 80LARC17C0004. Any opinions, findings, and conclusions or recommendations expressed in this material are those of the author(s) and do not necessarily reflect the views of the National Aeronautics and Space Administration.

The authors gratefully acknowledge the engineering team at LSTC for their willingness to work to improve the capabilities of the MAT261 material model.

References

[1] B. Justusson, J. Pang, M. Molitor, M. Rassaian and R. Rosman, "An Overview of the NASA Advanced Composites Consortium High Energy Dynamic Impact Phase II Technical Path," in *2019 AIAA/ Structures, Structural Dynamics, and Materials Conference*, San Diego, 2019.

[2] K. Hunziker, J. Pang, M. Melis, J. M. Pereira and M. Rassaian, "NASA ACC High Energy Dynamic Impact Methodology and Outcomes," in *2018 AIAA/ASCE/AHS/ASC Stuctures, Structural Dynamics, and Materials Conference*, Kissimmee, 2018.

[3] A. Byar, J. Pang, J. Iqbal, J. Ko and M. Rassaian, "Determination of Ballistic Limit for IM7/8552 Using LS-DYNA MAT261," in *AIAA SciTech Forum*, Kissimmee, 2018.

[4] B. Z. Gama, A Short Course on Progressive Composite Damage Modeling in LS-DYNA Using MAT162, Newark, DE: University of Delaware Center for Composite Materials, 2015.

[5] M. Molitor, B. Justusson, M. Rassaian and J. Pang, "Comparison of Test Methods to Determine Failure Parameters for MAT162 Calibration," in *2018 AIAA/ASCE/AHS/ASC Structures, Structural Dynamics, and Materials Conference*, Kissimmee, 2018.

[6] S. Hartmann, "Neue Materialmodelle für Composites in LS-DYNA," 17 April 2013. [Online]. Available: https://www.dynamore.de/en/downloads/infodays/dokumente/2013-composites/newmaterials.

[7] Livermore Software Technology Corporation, "LS-DYNA Keyword User's Manual - Volume 1," 2018.

[8] Livermore Software Technology Corporation, "LS-DYNA Keyword User's Manual - Volume 2, Material Models," 2018.

[9] H. Razi, J. Schaefer, S. Wanthal, J. Handler, G. Renieri and B. Justusson, "Rapid Integration of New Analysis Methods in Production," in *Proceedings of the American Society for Composites 31st Technical Conference*, Williamsburg, 2016.

[10] S. Wanthal, J. Schaefer, B. Justusson, I. Hyder, S. Engelstad and C. Rose, "Verification and Validation Process for Progressive Damage and Failure Analysis Methods in the NASA Advanced Composites Consortium," in *Proceedings from the American Society for Composites 32nd Technical Conference*, West Lafayette, 2017.

[11] S. Liguore, J. Schaefer, B. Justusson and M. Pike, "ONR High Fidelity Database and Validation Protocols for Structural Failure Mode Characterization - Program Highlights," in *Proceedings from the American Society for Composites 32nd Technical Conference*, West Lafayette, 2017.

[12] S. Pinho, C. Davila, P. Camanho, L. Iannucci and P. Robinson, "Failure Models and Criteria for FRP Under In-Plane or Three-Dimensional Stress States Including Shear Non-Linearity," NASA, Hampton, 2005.

[13] I. Hyder, J. Schaefer, B. Justusson, S. Wanthal, F. Leone and C. Rose, "Assessment of Intralaminar Progressive Damage and Failure Analysis Methods Using an Efficient Evaluation Framework," in *American Society for Composites (ASC) Annual Technical Conference*, West Lafaytte, 2017.

[14] B. Justusson, I. Hyder, S. Boyd and F. Leone, "Quantification of Error Associated with Using Misaligned Meshes in Continuum Damage Mechanics Material Models for Matrix Crack Growth Predictions in Composites," in *Proceedings of American Society for Composites 33rd Technical Conference*, Seattle, 2018.

[15] M. Melis, J. M. Pereira, R. Goldberg and M. Rassaian, "Dynamic Impact Testing and Model Development in Support of NASA's Advanced Composites Program," in *2018 AIAA/ASCE/AHS/ASC Structures, Structural Dynamics, and Materials Conference*, Kissimmee, 2018.

[16] ASTM D8101: Standard Test Method of Measuring Penetration Resistance of Composite Materials to Impact by a Blunt Projectile, West Conshohocken, PA: ASTM International, 2017.

[17] A. Manes, L. Peroni, M. Scapin and M. Giglio, "Analysis of Strain Rate Dependent Behavior of an Al 6061 T6 Alloy," *Prodedia Egnineering,* vol. 10, pp. 3477-3482, 2011.

[18] A. Selvarathinam, J. Action and B. Justusson, "Verification and Validation of Progressive Damage Analysis Methods for Explict Analysis of Progressive Delamination," in *American Society for Composites (ASC) 32nd Annual Technical Conference*, West Lafayette, 2017.